Strongly Stretched Polyelectrolyte Brushes

Christian Seidel*

Max-Planck-Institut für Kolloid- und Grenzflächenforschung,† Am Mühlenberg, D-14476 Golm, Germany

Received September 3, 2002

ABSTRACT: Using molecular dynamics simulations, we study completely and partially charged polyelectrolyte brushes. Counterions are treated explicitly. At weak electrostatic interaction we find that the collapsed brush regime obtained at strong interaction disappears. The chains become strongly stretched perpendicular to the grafting surface. Contrary to the well-known scaling law for the osmotic brush regime which gives a thickness, independent of grafting density, we obtain a weak, but nonvanishing, dependence. This unusual result is in agreement with the behavior in the *nonlinear osmotic brush regime* recently predicted on the basis of an extended theoretical model which includes the lateral inhomogeneity of counterion distribution.

1. Introduction

Polyelectrolytes have received a lot of attention in recent years because of their importance in biology, materials science, and soft matter research.[1] Polyelectrolyte brushes consist of charged polymers densely end-grafted to surfaces of various geometries.[2] Here we restrict ourself to the case of quenched polyelectrolytes end-tethered to a planar solid. Note that brushes of weak polyelectrolytes with an annealed charge distribution exhibit specific features.[3] Polyelectrolyte brushes form the subject of increasing interest by theory,[4−17] simulation,[16,18−22] and experiment.[23−30] Polyelectrolyte brushes are also interesting from the point of view of applications in colloid and material science: They are an efficient means for preventing colloids in polar media from flocculation.[31] The stabilization arising due to steric, entropic, and electrostatic repulsion is less sensitive to the salinity of the surrounding medium than a mechanism based on pure electrostatics (i.e., without polymers). A strongly charged brush is able to trap its own counterions and thus generates a layer of large effective ionic strength.[6] Recently, it has been shown that polyelectrolyte brushes can be successfully used in small devices such as porous filters for pH-controlled gating.[32] Similar to colloid stabilization, charged polymer brushes are thought to be a model of the envelope of cells. Living cells are surrounded by a kind of charged polymer layer (glycocalys) preventing nondesired protein−protein interaction.[33]

Both in experiment and in theoretical work, polyelectrolytes are an interesting subject with many unresolved problems. Simulations are a promising tool to check theoretical models and to probe quantities and regimes that are not easily observable experimentally.[34] However, despite strong effort in recent years,[35] simulations of polyelectrolytes remain still challenging. Because of the special methods required for treating the long-range Coulomb interaction, they are computational rather expensive.

In a previous simulation study,[22] we investigated the structure of completely charged polyelectrolyte brushes at relatively strong Coulomb interaction, setting the Bjerrum length $\lambda_B \approx 0.7b$ with b being the average bond length. In contrast to theoretical results,[6,7] which predict in the so-called osmotic regime a brush height independent of grafting density ρ_a, we observed a novel collapsed brush regime where the brush thickness grows linearly with ρ_a. Now it is understood that the collapsed brush regime can occur in the strong coupling limit $\lambda_B^3/\nu_2 > 1$ with ν_2 being the second virial coefficient.[16] On the other hand, up to now no collapsed behavior, related to correlation effects, has been reported in experiments, but experimental data have been evaluated to be in agreement with the osmotic brush regime.[27,28] This observation suggests that the experimental systems under consideration exhibit weak-coupling behavior, while previous simulations were dealing with a situation close to the strong-coupling case due to the particular setting of parameters.[16] Indeed, varying the Bjerrum length, we obtained a nonmonotonic behavior of the brush height with a maximum at rather small coupling strengths.[21] For a brush with completely charged chains of length $N = 20$, the behavior of the average height of chain ends $\langle z_e \rangle$ is shown in Figure 1. Together with the average height of the chain ends $\langle z_e \rangle$, we plotted the

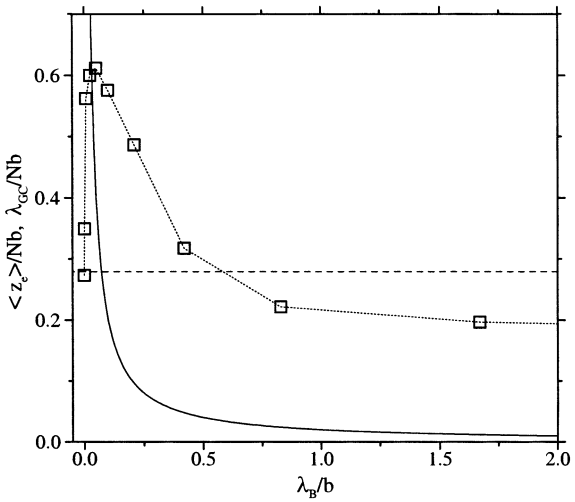

Figure 1. Average height of chain ends $\langle z_e \rangle$ (squares) and Gouy−Chapman length λ_{GC} (thick line), both rescaled with the contour length Nb ($N = 20$), vs Bjerrum length λ_B at grafting density $\rho_a\sigma^2 = 0.02$. The dashed line indicates $\langle z_e \rangle$ of an identical system of uncharged chains.

* E-mail: seidel@mpikg-golm.mpg.de.
† Mailing address: D-14424 Potsdam, Germany.

10.1021/ma021428g CCC: $25.00
Published on Web 03/13/2003

Gouy−Chapman length $\lambda_{GC} = (2\pi\lambda_B\Sigma)^{-1} = (2\pi\lambda_B f N\rho_a)^{-1}$, which is the height at which the counterions are effectively bound to a surface of charge density $e\Sigma = ef N\rho_a$.[6] Let us emphasize three points: (i) At Bjerrum lengths larger than about $0.5b$ the stretching of the chains is smaller than in a corresponding uncharged brush, indicating that attraction due to electrostatic correlations comes into play. (ii) The maximum brush height appears at $\lambda_B \lesssim 0.1b$. For smaller λ_B the Gouy−Chapman length becomes larger than the brush height. The counterions are expected to leave the brush, and the residual electrostatic repulsion between charged monomers is rather weak, leading to its relaxation back to the reduced extension of an quasi-neutral brush. (iii) Near the maximum height we obtain a stretching of the chains up to about $^2/_3$ of their contour length. This is certainly beyond the range where Gaussian elasticity can be applied.

Taking into account both the nonlinear elasticity of the chains and the lateral inhomogeneity of the counterion distribution, recently the osmotic brush regime has been reanalyzed by Naji et al.[17] Nonlinear elasticity is considered within the freely jointed chain model. In the large stretching limit $R \lesssim Nb$, the elastic free energy becomes $F_{elas}/k_BT \approx -N \log(1 - R/Nb)$, instead of the Gaussian law $F_{el}/k_BT \approx 3R^2/2Nb^2$, which is correct in the limit of small stretching $R \ll Nb$. However, it is known that finite extensibility alone does not change the scaling behavior of brush height with grafting density.[13] Nevertheless, it is important for the comparison of theory with simulation data as well as experimental ones because at large stretching it strongly influences the absolute value of chain extension.

In ref 14, the nonlinear Poisson−Boltzmann equation has been solved without any assumption about the distribution of the counterions perpendicular to the grafting surface. It has been shown that the brush height grows monotonically with grafting density when the counterion distribution extends beyond the rim of the brush. In the limit of large Gouy−Chapman length $\lambda_{GC} \gg h_{OsB}$, with h_{OsB} being the brush height in the osmotic regime, one obtains the so-called Pincus brush[6] with a brush height $h_{PB} \sim N^3b^2f^2\lambda_B\rho_a$. On the other hand, the osmotic regime with $h_{OsB} \sim Nbf^{1/2}$ is recovered in the limit $\lambda_{GC} \ll h_{OsB}$. In ref 14 as well as in all previous theoretical studies, it was commonly assumed that counterions are distributed uniformly in the lateral directions parallel to the grafting plane. However, an inhomogeneous distribution was obtained in both simulation[16,22] and experiment.[30] Using nonlinear Poisson−Boltzmann theory, lateral inhomogeneity is explicitly taken into account in ref 17. It was shown there that lateral inhomogeneity of the counterion distribution yields a weak dependence of brush height on anchoring density although the counterions are assumed to be trapped inside the brush. The corresponding brush regime is called *nonlinear osmotic*.

The aim of this paper is to study the behavior of polyelectrolyte brushes at rather weak Coulomb interaction. To reach the weak-coupling limit, the Bjerrum length is set $\lambda_B \approx 0.1b$. The parameters of the underlying neutral chain are not changed compared to previous simulations with $\lambda_B \approx 0.7b$. Hence, any feature of the collapsed regime is expected to disappear, but the polyelectrolyte chains should exhibit strong stretching.

The paper is organized as follows. In the next section we introduce the polyelectrolyte model and the simulation technique. The results obtained for completely and partially charged brushes are discussed in section 3. Conclusions are given in section 4.

2. Simulation Model and Method

The brush is represented by M freely jointed bead−spring chains of length $N + 1$ which are anchored by one end to an uncharged surface at $z = 0$. The chains are assumed to be in a good solvent modeled by a repulsive short-range interaction which is described by a shifted Lennard-Jones potential

$$u_{LJ}(r) = \begin{cases} 4\epsilon\left\{\left(\frac{\sigma}{r}\right)^{12} - \left(\frac{\sigma}{r}\right)^{6} + \frac{1}{4}\right\}, & \text{if } r < r_c \\ 0, & \text{if } r \geq r_c \end{cases} \quad (1)$$

where the cutoff radius is $r_c = 2^{1/6}\sigma$ and ϵ, σ are the usual Lennard-Jones parameters. For simplicity, we assume that both monomers and counterions are interacting with the same shifted Lennard-Jones potential, i.e., $\sigma_m = \sigma_{ci} = \sigma$ and $\epsilon_m = \epsilon_{ci} = \epsilon$. Henceforth, ϵ and σ are used as basic units of the model. In addition to the repulsive potential, beads being neighbors along the polymer chains are coupled by a FENE (finite extensible nonlinear elastic) bond potential[34]

$$u_{bond}(r) = \begin{cases} -\frac{kR_0^2}{2}\log\left\{1 - \left(\frac{r}{R_0}\right)^2\right\}, & \text{if } r < R_0 \\ \infty, & \text{if } r \geq R_0 \end{cases} \quad (2)$$

with bond strength $k = 30\epsilon/\sigma^2$ and maximum bond length $R_0 = 1.5\sigma$. For completely charged chains, this choice of parameters gives an average bond length of $b = 0.98\sigma$, which fluctuates by about 4%.[22] The Coulomb repulsion between adjacent monomers slightly stretches the bond length compared to uncharged chains, where $b = 0.97\sigma$ has been reported.[36] Within the simulation box of size $L \times L \times L_z$ the grafting density is given by $\rho_a = M/L^2$. The uncharged anchor segments are fixed and form a square lattice with lattice spacing $d = \rho_a^{-1/2}$. All particles except the anchor segments interact repulsively with the grafting surface at short distances. The exact form of the wall potential is arbitrary. In principle, one can use any strongly repelling short-range potential. Here we use a potential similar to the shifted Lennard-Jones potential introduced in eq 1 which vanishes smoothly as $z \to 0.5\sigma$

$$u_{wall}(z) = \begin{cases} 4\epsilon\left\{\left(\frac{\sigma}{z + \Delta z}\right)^{12} - \left(\frac{\sigma}{z + \Delta z}\right)^{6} + \frac{1}{4}\right\}, & \text{if } z < 0.5\sigma \\ 0, & \text{if } z \geq 0.5\sigma \end{cases} \quad (3)$$

with $\Delta z = (2^{1/6} - 0.5)\sigma$. Counterions are treated as individual, nonbonded particles. To prevent divergences at large Gouy−Chapman lengths, in addition to the repulsive wall potential at the $z = 0$ plane, a similar potential is assigned to the top boundary of the simulation box. However, to guarantee that this restriction is only a small perturbation, L_z has to be chosen large enough that collisions of counterions with the top plane of the simulation box remain rare events. In the simulations reported here we used $L_z = 3N\sigma$. For completely charged chains ($f = 1$), this choice ensures that $\lambda_{GC}/L_z \ll 1$ and counterions never visit the $z = L_z$ boundary in the course of the simulations. All the

charged entities interact with the bare Coulomb interaction

$$u_{\mathrm{Coul}}(r) = k_{\mathrm{B}}T q_i q_j \frac{\lambda_{\mathrm{B}}}{r} \tag{4}$$

with q_i and q_j being the corresponding charges in units of elementary charge e. The Bjerrum length which determines the strength of Coulomb interaction is given by $\lambda_{\mathrm{B}} = e^2/(4\pi\varepsilon_0\varepsilon k_{\mathrm{B}}T)$, where ε_0 and ε are the vacuum permittivity and the dielectric constant of the solvent, respectively. The calculation of long-ranged Coulomb interaction in periodic systems requires special care. In the problem under consideration we have periodic boundary conditions only in two dimensions (x and y) while perpendicular to the grafting surface (z-direction) the system is restricted to one layer. To calculate Coulomb forces and energies in the case of a 2D+1 slab geometry, we use a technique proposed by Lekner[37] and modified by Sperb.[38] Details of the implementation can be found in ref 22. We assume that we have a system with matching ε boundary condition, so that no image charges appear across the anchoring surface. For highly charged and densely grafted systems, image charge effects are indeed expected to be small.[10]

To study the system in equilibrium, we use stochastic molecular dynamics.[39,40] The equation of motion for particle i at position $\mathbf{r}_i(t)$ is the Langevin equation

$$m\frac{\mathrm{d}^2\mathbf{r}_i}{\mathrm{d}t^2} = -\nabla_i U - m\Gamma\frac{\mathrm{d}\mathbf{r}_i}{\mathrm{d}t} + \mathbf{W}_i(t) \tag{5}$$

where all particles carry the same mass m and Γ is a friction constant which couples the particles to a heat bath. U is the potential energy

$$U = U_{\mathrm{LJ}} + U_{\mathrm{bond}} + U_{\mathrm{wall}} + U_{\mathrm{Coul}} \tag{6}$$

The system is held at thermal equilibrium by a Gaussian random force $\mathbf{W}_i(t)$

$$\langle \mathbf{W}_i(t) \rangle = 0$$

$$\langle \mathbf{W}_i(t)\cdot\mathbf{W}_j(t') \rangle = 6m k_{\mathrm{B}}T\Gamma\delta_{ij}\delta(t - t') \tag{7}$$

where the coupling to Γ is a consequence of the fluctuation−dissipation relation.

We used $m = 1$, $k_{\mathrm{B}}T = 1.2\epsilon$, and $\Gamma = 0.5\tau_{\mathrm{LJ}}{}^{-1}$ with $\tau_{\mathrm{LJ}} = \sqrt{m\sigma^2/\epsilon}$ being the Lennard-Jones time unit. Equation 5 was integrated by means of the velocity−Verlet algorithm[40] with a time step $\delta t = 0.006\tau_{\mathrm{LJ}}$. For a Newtonian trajectory with a quite similar time step, the total energy fluctuations have shown to be less than 10^{-4}.[22]

The molecular dynamics code was parallelized using a self-scheduling (master-slave) algorithm[41] for the force loop. Upon testing the parallel code for different processor numbers n, we found that the efficiency is optimal in the range of $n = 32$ to $n = 64$ processors, where an efficiency of over 90% is reached. Lower numbers of processors lead to a loss in efficiency due to the idle master processor, while large processor numbers are less efficient because communication time becomes a dominant contribution. It should be noted that the efficiency of the parallel code strongly depends on the degree of charging. Therefore, it is only used for simulating strongly charged polyelectrolytes. Weakly charged systems are studied by using the sequential version of the code on local compute servers with Alpha EV67/667 processors.

If not otherwise stated, in this study we have considered systems with $M = 36$ polyelectrolyte chains, each consisting of an uncharged fixed anchor and $N = 30$ free chain monomers, $f \times N$ of which are (negatively) charged. The degree of charging f varies between one (completely charged) and zero (neutral). Because of electroneutrality, there are $f \times M \times N$ counterions. Two types of finite size effects may interfere with the simulation results discussed below. First, the chain length N should be long enough to capture typical polymeric behavior. Second, because of possible self-interaction of the chains, a small lateral system size due to the restricted number of chains M may also influence the large-scale properties such as brush thickness. Although we cannot completely rule out that finite size effects will still have an effect on the simulation results discussed below (in particular on the prefactors of the scaling laws), in ref 22 it has been shown that at the particular system size, used also in the present study, both types of finite size effects can be kept small. Note that at $f = 1$ the system contains 2160 charged particles. Such simulations imply CPU times that require the use of parallel supercomputers.

For strongly charged chains, the anchoring density ρ_{a} varies between $0.042\sigma^{-2}$ and $0.120\sigma^{-2}$, which corresponds to a box size L between 29.3σ and 17.3σ. For these systems, λ_{GC} ranges from 1.3σ down to 0.5σ. That is why most of the counterions are expected to be still confined in the brush. On the other hand, this means that the stretching of the chains is still below its maximum. To reach the asymptotic limit of a neutral brush, for weakly charged chains, an additional anchoring density is studied with $L = 15.5\sigma$ or $\rho_{\mathrm{a}} = 0.15\sigma^{-2}$. Fully stretched chains with a line of counterions were used as initial configuration. The relaxation was monitored by studying the decay of the end-point height of the chains. Details of the equilibration procedure can be found elsewhere.[22] Typically, the relaxation of the brushes takes some hundreds of τ_{LJ}. After reaching equilibrium, we calculated trajectories between $2500\tau_{\mathrm{LJ}}$ and $4000\tau_{\mathrm{LJ}}$, depending on degree of charging and anchoring density. With this trajectory lengths one can ensure that the relative error of the average height of chain ends is less than 0.5%, which has been proved to be sufficient for obtaining smooth end-point distribution functions. Errors were estimated by computing block averages[40] and by monitoring cumulative averages.[42]

We have to note that with the setting $\lambda_{\mathrm{B}} = 0.1\sigma$ the direct mapping of the coarse-grained model to the standard experimental system; i.e., fully charged poly(styrenesulfonate) (PSS) is lost. Because the length scale of the model is set by the Bjerrum length, which is about 0.7 nm for water at room temperature, the bond length (i.e., the average distance between neighboring charges along the chain at $f = 1$) becomes $b \approx 7$ nm. Using for PSS a monomer size of about 0.25 nm, one results with a fraction of charged monomer $f \approx 1/30$, which is 1 order of magnitude below the value known for standard PSS. However, the model could be mapped to weakly charged PSS which can be produced by controlled sulfonation from polystyrene standards.[43] On the other hand, there are experimental systems that exhibit inherently much larger average distances between neighboring charges. For, e.g., poly(methacrylic acid), which is a weak poly-

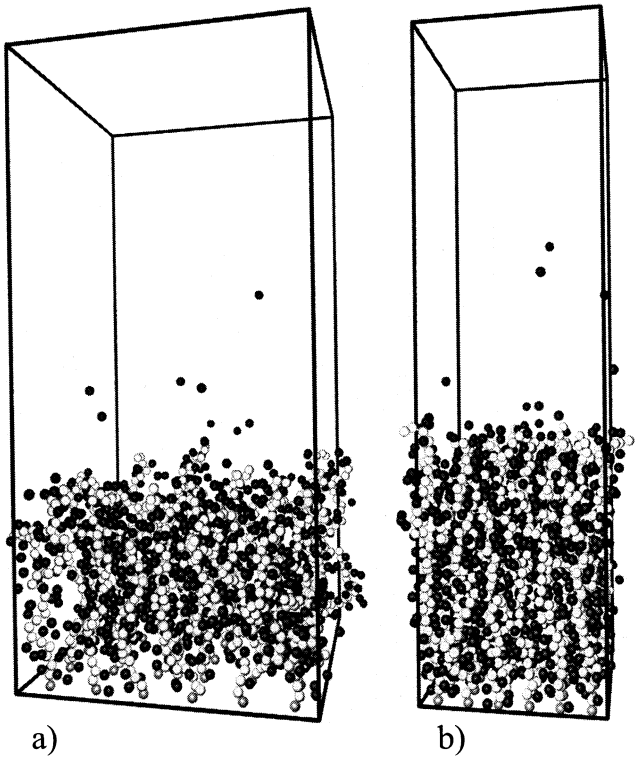

Figure 2. Polyelectrolyte brushes with $M = 36$ chains of length $N = 30$, completely charged at grafting density (a) $\rho_a\sigma^2 = 0.042$ and (b) $\rho_a\sigma^2 = 0.120$. The Bjerrum length is $\lambda_B = 0.1\sigma$. Counterions are assigned to the closest polyelectrolyte chain; polyelectrolyte chains are light gray, counterions are black, and anchor monomers are dark gray. The box height perpendicular to the grafting surface has been reduced for the sake of representation. Snapshots have been represented by using the visualization program VMD.[44]

electrolyte with annealed charge distribution, under certain conditions the average distance is about 10 nm.[29] Thus, the coarse-grained model with the parameter settings chosen here can be applied to real systems. Let us remember that the reason for choosing $\lambda_B = 0.1\sigma$ was to enter the weak-coupling region $\lambda_B < {v_2}^{1/3}$. To compare the theoretical model with the simulations, however, the second virial v_2 has been estimated in a very crude way.[16] To allow an appropriate consideration of real systems, doubtless a more sophisticated way for evaluating v_2 is required.

3. Simulation Results and Discussion

3.1. Structure of the Brush. Figure 2 shows snapshots from the equilibrium trajectories of completely charged brushes at the smallest and largest grafting density considered in the study. In this representation, the connectivity of the chains has been preserved, such that the chains may extend beyond the simulation box. The counterions are assigned to the closest chain monomer. Considering the snapshots, we address two points: (i) Immediately one can realize that the chains become strongly stretched and aligned perpendicular to the grafting surface. (ii) As expected from the estimation of the Gouy−Chapman length, in the case of completely charged brushes almost all the counterions remain trapped inside the brush. Both features will be quantitatively discussed below.

For completely charged brushes, Figure 3 gives the monomer density $\rho_m(z)$ as a function of the distance from the grafting surface. $\rho_m(z)$ is normalized such that $\int_0^\infty dz$

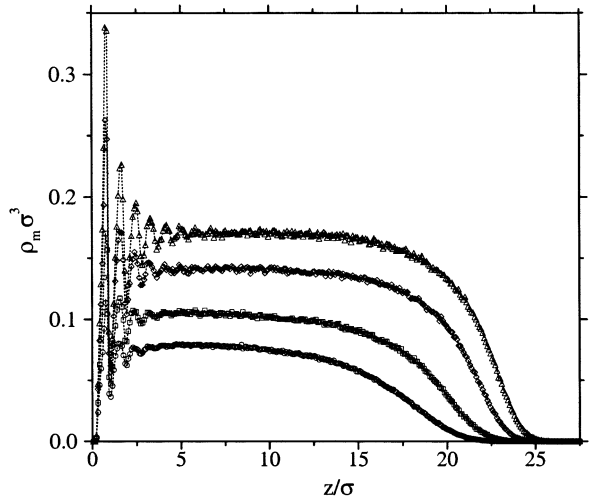

Figure 3. Monomer density profiles $\rho_m(z)$ of completely charged polyelectrolyte brushes ($N = 30$, $\lambda_B = 0.1\sigma$) as a function of the distance from the grafting surface. Shown are four different anchoring densities $\rho_a\sigma^2 = 0.042$ (circles), $\rho_a\sigma^2 = 0.063$ (squares), $\rho_a\sigma^2 = 0.094$ (diamonds), and $\rho_a\sigma^2 = 0.120$ (triangles).

$\rho_m(z) = N\rho_a$. Let us remember that in the collapsed regime, obtained in the strong coupling limit, the monomer density becomes independent of anchoring density, resulting in a linear scaling of brush height with anchoring density.[16,22] Obviously, at $\lambda_B = 0.1\sigma$ there remain no reminiscences of such a behavior. The extension of the brushes is substantially increased, and its dependence on anchoring density becomes much weaker.

The average thickness of the brush and of the counterion layer is measured by taking the first moments of the corresponding density profiles:

$$\langle z_m \rangle = \frac{\int_0^\infty z\rho_m(z)\,dz}{\int_0^\infty \rho_m(z)\,dz}, \quad \langle z_{ci} \rangle = \frac{\int_0^\infty z\rho_{ci}(z)\,dz}{\int_0^\infty \rho_{ci}(z)\,dz} \tag{8}$$

Note that a possible logarithmic divergence in the first moment of the counterion density at large λ_{GC} due to the $1/z^2$ decay of $\rho_{ci}(z)$ is canceled by the finite size of the simulation box in the z-direction. The term neglected by closing the system is of the order of $A \log(L_z/\lambda_{GC})$ with a prefactor $A \ll 1$. A systematic simulation study of the behavior of counterions at charged plates in both open and closed systems can be found in ref 45.

The average monomer and counterion heights for all systems studied with $\lambda_B = 0.1\sigma$, completely and partially charged ones, are given in Table 1. For completely charged brushes the comparison with the previously studied strong coupling case $\lambda_B = 0.7\sigma$[22] is shown in Figure 4. As indicated by the snapshots shown in Figure 2, at $f = 1$ most of the counterions remain still captured inside the brush, and the relation between $\langle z_m \rangle$ and $\langle z_{ci} \rangle$ is not perceptibly changed compared to the behavior obtained at strong coupling $\lambda_B = 0.7\sigma$. With an exponent $\alpha = {}^1/_5$ there appears a rather weak dependence on anchoring density. However, contrary to the well-known scaling law for charged brushes in the osmotic regime, which predicts a thickness independent of the anchoring density, there remains a weak, but nonnegligible, dependence on ρ_a.

Table 1. Simulation Results: Average Brush Height $\langle z_m \rangle$, Average Counterion Height $\langle z_{ci} \rangle$, and Average End-Point Height $\langle z_e \rangle$ at Different Grafting Density ρ_a and Degree of Charging f [a]

$\rho_a\sigma^2$	f	$\langle z_m \rangle/\sigma$	$\langle z_{ci} \rangle/\sigma$	$\langle z_e \rangle/\sigma$
0.042	1	8.72 ± 0.01	9.16 ± 0.01	15.74 ± 0.03
0.042	1/2	7.66 ± 0.01	8.01 ± 0.01	13.33 ± 0.03
0.042	1/3	7.08 ± 0.01	7.69 ± 0.01	12.24 ± 0.03
0.042	1/5	6.38 ± 0.01	7.65 ± 0.02	10.83 ± 0.03
0.042	1/10	5.72 ± 0.01	8.36 ± 0.02	9.61 ± 0.03
0.042	1/15	5.48 ± 0.01	9.04 ± 0.03	9.09 ± 0.03
0.042	1/30	5.27 ± 0.01	11.08 ± 0.07	8.58 ± 0.03
0.042	0	5.12 ± 0.01		8.09 ± 0.03
0.063	1	9.48 ± 0.01	9.94 ± 0.01	17.54 ± 0.03
0.063	1/2	8.17 ± 0.01	8.46 ± 0.01	14.45 ± 0.03
0.063	1/3	7.52 ± 0.01	8.17 ± 0.01	13.18 ± 0.03
0.063	1/5	6.76 ± 0.01	7.94 ± 0.02	11.67 ± 0.03
0.063	1/10	6.14 ± 0.01	8.82 ± 0.02	10.53 ± 0.03
0.063	1/15	5.90 ± 0.01	9.42 ± 0.04	10.02 ± 0.03
0.063	1/30	5.75 ± 0.01	11.90 ± 0.07	9.51 ± 0.03
0.063	0	5.58 ± 0.01		9.06 ± 0.03
0.094	1	10.30 ± 0.01	10.77 ± 0.01	19.57 ± 0.02
0.094	1/2	8.85 ± 0.01	9.12 ± 0.01	15.99 ± 0.03
0.094	1/3	8.13 ± 0.01	8.69 ± 0.01	14.50 ± 0.03
0.094	1/5	7.40 ± 0.01	8.58 ± 0.001	13.04 ± 0.03
0.094	1/10	6.73 ± 0.01	9.51 ± 0.02	11.82 ± 0.03
0.094	1/15	6.54 ± 0.01	10.18 ± 0.03	11.36 ± 0.02
0.094	1/30	6.33 ± 0.01	13.00 ± 0.07	10.69 ± 0.02
0.0940	0	6.23 ± 0.01		10.36 ± 0.03
0.120	1	10.78 ± 0.01	11.25 ± 0.01	20.64 ± 0.02
0.120	1/2	9.26 ± 0.01	9.50 ± 0.01	16.87 ± 0.03
0.120	1/3	8.51 ± 0.01	9.10 ± 0.01	15.32 ± 0.03
0.120	1/5	7.83 ± 0.01	9.01 ± 0.01	13.95 ± 0.02
0.120	1/10	7.18 ± 0.01	9.94 ± 0.02	12.74 ± 0.03
0.120	1/15	7.00 ± 0.01	10.75 ± 0.03	12.30 ± 0.02
0.120	1/30	6.81 ± 0.01	13.41 ± 0.06	11.67 ± 0.03
0.120	0	6.69 ± 0.01		11.33 ± 0.03
0.150	1/5	8.20 ± 0.01	9.87 ± 0.01	14.93 ± 0.02
0.150	1/10	7.65 ± 0.01	10.51 ± 0.02	13.68 ± 0.02
0.150	1/15	7.45 ± 0.01	11.53 ± 0.03	13.19 ± 0.02
0.150	1/30	7.26 ± 0.01	14.09 ± 0.05	12.63 ± 0.03
0.150	0	7.17 ± 0.01		12.35 ± 0.02

[a] The Bjerrum length is $\lambda_B \approx 0.1b$.

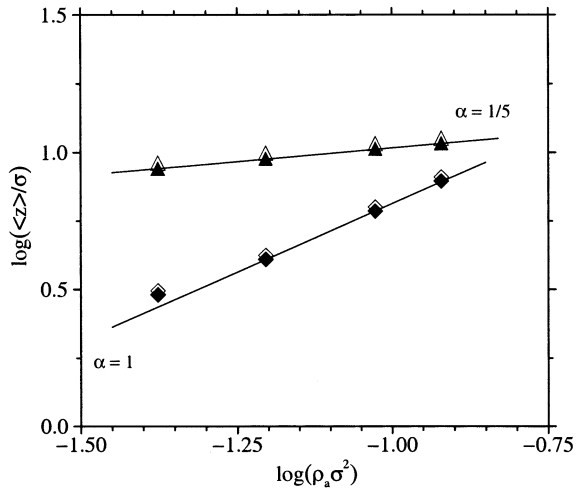

Figure 4. Average brush height $\langle z_m \rangle$ (filled symbols) and average counterion height $\langle z_{ci} \rangle$ (empty symbols) of completely charged polyelectrolyte brushes vs anchoring density both for $\lambda_B = 0.7\sigma$ (diamonds)[22] and $\lambda_B = 0.1\sigma$ (triangles). Error bars are smaller than symbol size.

At first sight, it was unclear whether this unusual behavior might be only a feature of a crossover regime that appears accidentally due to the particular parameters chosen in the simulations. At least for completely charged brushes, there is no way to explain the dependence of the brush thickness on grafting density due to the transverse distribution of counterions. Most of them are still trapped inside the brush, and only a few percent are free to leave (see Figure 2 and Table 1). Note that the dimensionless parameter h_{OsB}/λ_{GC}, governing the dependence of the brush thickness on grafting density in the model proposed by Zhulina and Borisov,[14] is rather large (of the order of 10), indicating a behavior similar to the osmotic brush. Now it is understood that a dependence of the brush thickness on grafting density can be also caused by a lateral inhomogeneity of the counterion density[17] which is more likely to explain the simulation data under discussion. In the model used by Naji et al. the electrostatic free energy is evaluated within the cylinder model by means of nonlinear Poisson−Boltzmann theory. The elastic free energy of the chains is treated using a freely jointed chain model and the short-range volume interaction is included by imposing a constant volume constraint for the polyelectrolyte. Doing so, reasonable agreement between simulation data and theoretical predictions has been obtained without any fitting parameter in the so-called *nonlinear osmotic brush regime*.[17] Independently, recent experimental data indicate also a weak dependence of the brush height on anchoring density.[46]

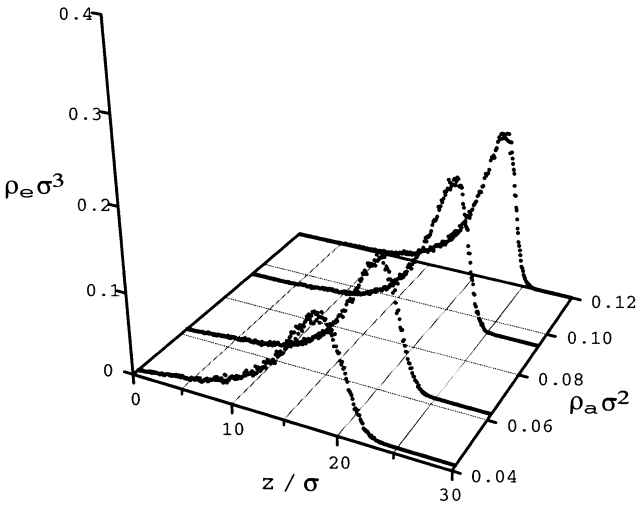

Figure 5. End-point distributions of completely charged polyelectrolyte brushes at weak coupling $\lambda_B = 0.1\sigma$. Grafting densities are the same as in Figure 3.

Figure 5 gives the end-point distribution $\rho_e(z)$ normalized to unity. One notes that, for all grafting densities ρ_a, the end-point distribution exhibits a pronounced peak at large z and decays strongly inside the brush. These features reflect the highly ordered brush state due to strong stretching perpendicular to the grafting surface. The behavior is in contrast to that found in the collapsed brush regime at low grafting densities,[22] where a second peak of the end-point distribution was obtained at small z, indicating that the chains are likely to fold back onto the surface.

For a more detailed examination of the intrachain structure of grafted polyelectrolytes at all length scales, we calculate the spherically averaged single chain structure factor

$$S(q) = \left\langle \left\langle \frac{1}{N+1} \left| \sum_{j=0}^{N} \exp(i\mathbf{q}\cdot\mathbf{r}_j) \right|^2 \right\rangle_{|\mathbf{q}|} \right\rangle \qquad (9)$$

as well as the structure factor in transverse direction $S(q_z)$ and the in-plane averaged one $S(q_{xy})$. In analogy

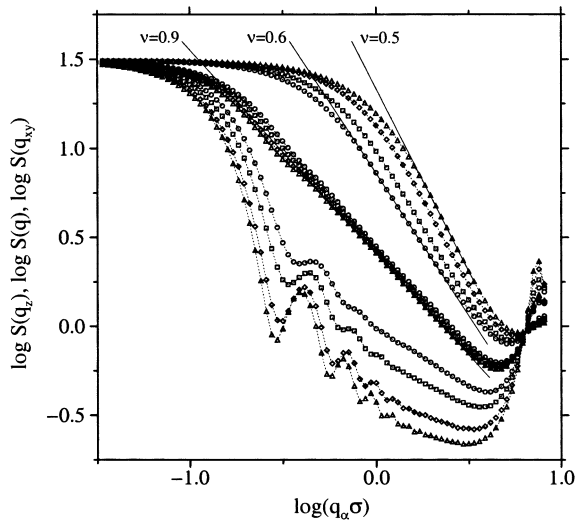

Figure 6. Spherically averaged structure factor $S(q)$ (middle set), in-plane averaged structure factor $S(q_{xy})$ (upper set), and structure factor perpendicular to the grafting plane $S(q_z)$ (lower set) of completely charged polyelectrolyte brushes at $\lambda_B = 0.1\sigma$. Grafting densities and symbols are the same as in Figure 3.

to free chains, in the asymptotic regime the structure factor is expected to obey the scaling relation $S(q) \sim q^{-1/\nu}$, where ν is the exponent of the N dependence of the chain radius $R \sim N^{\nu}$. Figure 6 gives the three different structure factors. Within the range of the anchoring densities studied in the simulations, the spherically averaged structure factor $S(q)$ is almost not changed, reflecting strong stretching with a exponent $\nu \approx 0.9$. This result is consistent with the structure perpendicular to the grafting plane, shown by $S(q_z)$ which exhibits strong features of a rigid-rod-like behavior amplified with increasing anchoring density. Note that a highly ordered layering evolves close to the grafting surface. The transverse monomer profiles shown in Figure 3 indicate short-range ordering in a stack ranging from three up to seven layers above the grafting surface. The most interesting additional information gives the in-plane averaged structure factor $S(q_{xy})$. Note that the in-plane behavior of the grafted polyelectrolyte chains is determined by the properties of the underlying neutral chains. In agreement with our model, which is supposed to mimic polyelectrolytes under good-solvent conditions, at low grafting densities $S(q_{xy})$ gives an in-plane scaling $R_{xy} \sim N^{0.6}$. At large ρ_a, however, $S(q_{xy})$ indicates $R_{xy} \sim N^{0.5}$, i.e., the scaling behavior of a Gaussian chain well-known for chains in melt.

3.2. Counterion Distribution. In refs 16 and 22 it has been shown that the particular behavior of polyelectrolyte brushes in the strong-coupling limit, i.e., the existence of a collapsed regime, is caused by Coulomb correlations. To discuss the role of correlations and the degree of counterion condensation, we calculated the ion−polyelectrolyte distribution function $p(r)$ where r is the separation between counterion center and closest polyelectrolyte bond. The distribution $p(r)$ is normalized according to $2\pi \int_0^\infty rp(r)\,dr = 1$. For strong coupling, at $\lambda_B = 0.7\sigma$, the distribution functions show a pronounced peak at $r = \sigma$.[22] At $\lambda_B = 0.1\sigma$, the peak is much weaker and the probability remains finite up to larger distances (see Figure 7). There is still another remarkable difference between the two situations: At strong interaction strength the lowest anchoring density shows the highest

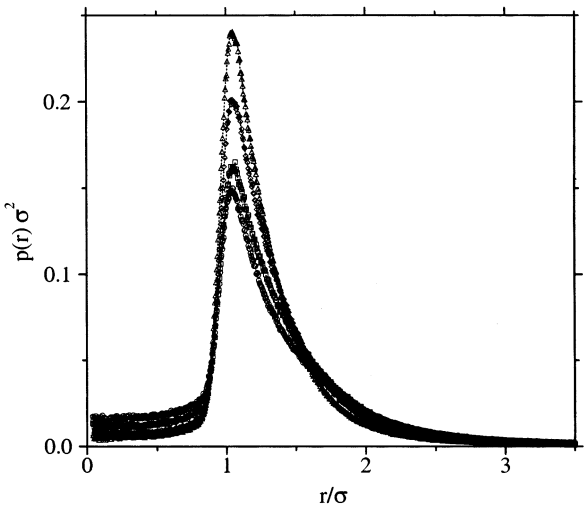

Figure 7. Ion−polyelectrolyte distribution function for completely charged chains at $\lambda_B = 0.1\sigma$. Grafting densities and symbols are the same as in Figure 3.

peak value. This can be understood due to the decreasing effective line charge density $N/2\langle z_m\rangle$ with increasing stretching of the chain, i.e., with increasing anchoring density. Thus, the effective Manning ration $\xi_{eff} = N\lambda_B/2\langle z_m\rangle$ exhibits its largest value at the lowest anchoring density, giving rise for a large fraction of "condensed" counterions. On the other hand, at weak interaction the peak becomes monotonically enhanced with growing anchoring density, which is probably a simple packing effect.

3.3. Partially Charged Brushes. Considering partially charged chains, once more we observe quite different behavior at strong and weak interaction strengths. In Figure 8 the scaling behavior of the brush height as a function of grafting density is plotted for different degree of charging f.

At $\lambda_B = 0.7\sigma$, previously we found a nonmonotonic behavior:[16] At large ρ_a the brush shrinks with decreasing f, while at small grafting density unexpectedly the brush is expanding with a reduced degree of charging. The particular behavior at small grafting densities is consistent, however, with the predictions of the collapsed brush regime where the brush height scales as $h \sim 1/f^3$. At high anchoring densities steric repulsion of monomers and counterions becomes dominant and gives rise to the growing of brush height with ρ_a. The quasi-neutral brush regime is reached at a small, but finite, degree of charging.

On the other hand, at $\lambda_B = 0.1\sigma$ we obtain a completely monotonic behavior. Reducing the degree of charging the brush shrinks at any grafting density. However, any finite charge on the chain (together with the corresponding counterions) gives rise to an additional stretching of the brush compared to the uncharged one, and the limiting scaling law $h \sim \rho_a^{1/3}$ is attained only at very small f.

Note that for weakly charged brushes the Gouy−Chapman length becomes rather large, and a substantial fraction of counterions leave the brush. Obviously, the influence of the inhomogeneity in the transverse distribution of counterions cannot be neglected in this case, but the crossover in the dependence of the brush thickness on grafting density involves a complex interplay between second virial effects and inhomogeneities in all spatial directions.

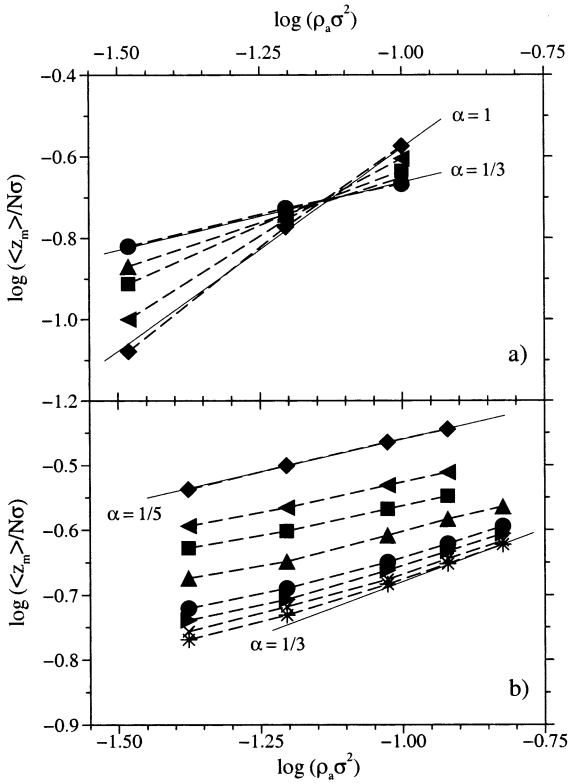

Figure 8. Brush height $\langle z_m \rangle$ of completely and partially charged chains vs anchoring density ρ_a: (a) $\lambda_B = 0.7\sigma$, $N_1 = 50$[16] and (b) $\lambda_B = 0.1\sigma$, $N_2 = 30$. $f = 1$ (diamonds), $f = 1/2$ (triangle left), $f = 6/25$ (N_1) or $f = 1/3$ (N_2) (squares), $f = 4/25$ (N_1) or $f = 1/5$ (N_2) (triangles up), $f = 2/25$ (N_1) or $f = 1/10$ (N_2) (circles), $f = 1/15$ (triangles right), $f = 1/30$ (cross) and $f = 0$ (star). The limiting power laws ρ_a^1, $\rho_a^{1/3}$, and $\rho_a^{1/5}$ are given as a guide to the eyes.

4. Conclusion

Performing extensive simulation of completely and partially charged polyelectrolytes, we have shown that the collapsed brush regime found at strong Coulomb interaction disappears when the interaction strength is reduced. The substantial difference between strong and weak interaction is also reflected in the counterion distribution and in the specific behavior of partially charged brushes.

We obtain strong stretching of the chains that reaches, at the maximum, an end-to-end distance of about $^2/_3$ of the contour length. For such brushes, contrary to the well-known scaling law for the osmotic brush regime, which predicts a thickness independent of grafting density ρ_a, we obtain a weak, but nonvanishing, dependence of the brush height on ρ_a. It is known[14] that a grafting density dependence occurs when the counterion distribution extends beyond the rim of the brush, as this reduces both the osmotic pressure exerted by counterions and the screening of the Coulomb interaction inside the brush. But, such a mechanism can be ruled out in our case because almost all the counterions have been found to be trapped within the brush. However, contrary to the assumption made in theoretical models of polyelectrolyte brushes, we observe a strong lateral inhomogeneity in the counterion distribution which was also obtained in experimental studies. In a recent theoretical study,[17] it has been shown that such an inhomogeneity can also produce a weak dependence of the brush thickness on grafting density, a regime which has been called *nonlinear osmotic*. In fact, including lateral inhomogeneity of the counterion distribution together with nonlinear elasticity of the polyelectrolyte chains provides reasonable agreement between simulation data and theoretical predictions without any fitting parameters.[17]

From an experimental point of view, tethering charged chains by an end at a surface is a rather challenging task which can be only solved with relatively short polymers. Therefore, the finite extensibility and, related to that, the nonlinear elasticity of the chains can play an important role in the brush regime. On the other hand, an inhomogeneous counterion distribution in the lateral direction has been reported in recent experiments.[30] Therefore, both effects, i.e., nonlinear elasticity and lateral inhomogeneity, neglected in scaling approaches might play an important role in experimental systems. Interestingly, there is some indication on a weak dependence of the chain stretching on anchoring density from recent experiments with polyelectrolyte brushes.[46]

We conclude the following: (i) It is necessary to evaluate a more sophisticated parameter mapping between experimental systems and the coarse-grained theoretical model applied also in simulations. (ii) It would be very useful to have more experimental data on the structure of diversified polyelectrolyte brushes in different environment in order to check the relevance of theoretical models and related simulation studies.

Acknowledgment. This work was supported by the Deutsche Forschungsgemeinschaft within the Schwerpunktprogramm Polyelektrolyte. We gratefully acknowledge grants for computer time at the John von Neumann-Institut for Computing (NIC) Jülich and the Konrad Zuse Zentrum für Informationstechnik Berlin (ZIB). I also thank Roland Netz, Ali Naji, and Oleg Borisov for useful discussions.

References and Notes

(1) Dautzenberg, H.; Jaeger, W.; Kötz, J.; Philipp, B.; Seidel, C.; Stscherbina, D. *Polyelectrolytes: Formation, Characterization and Application*; Hanser Publishers: Munich, 1994. Förster, S.; Schmidt, M. *Adv. Polym. Sci.* **1995**, *120*, 51−133. Barrat, J.-L.; Joanny, J.-F. *Adv. Chem. Phys.* **1996**, *94*, 1−66.
(2) Halperin, A.; Tirrell, M.; Lodge, T. P. *Adv. Polym. Sci.* **1991**, *100*, 31−71. Guenoun, P.; Argillier, J.-F.; Tirrell, M. *C. R. Acad. Sci. Paris, Ser. IV* **2000**, *1*, 1163−1169.
(3) Israëls, R.; Leermakers, F. A. M.; Fleer, G. J. *Macromolecules* **1994**, *27*, 3087−3093.
(4) Miklavic, S. J.; Marčelja, S. *J. Phys. Chem.* **1988**, *92*, 6718−6722.
(5) Misra, S.; Varanasi, S.; Varanasi, P. P. *Macromolecules* **1989**, *22*, 4173−4179.
(6) Pincus, P. *Macromolecules* **1991**, *24*, 2912−2919.
(7) Borisov, O. V.; Birstein, T. M.; Zhulina, E. B. *J. Phys. II* **1991**, *1*, 521−526.
(8) Ross, R. S.; Pincus, P. *Macromolecules* **1992**, *25*, 2177−2183.
(9) Zhulina, E. B.; Birstein, T. M.; Borisov, O. V. *J. Phys. II* **1992**, *2*, 63−74.
(10) Wittmer, J.; Joanny, J.-F. *Macromolecules* **1993**, *26*, 2691−2697.
(11) Israëls, R.; Leermakers, F. A. M.; Fleer, G. J.; Zhulina, E. B. *Macromolecules* **1994**, *27*, 3249−3261.
(12) Borisov, O. V.; Zhulina, E. B.; Birshtein, T. M. *Macromolecules* **1994**, *27*, 4795−4803.
(13) Amoskov, V. M.; Pryamitsyn, V. A. *J. Chem. Soc., Faraday Trans.* **1994**, *90*, 889−893.
(14) Zhulina, E. B.; Borisov, O. V. *J. Chem. Phys.* **1997**, *107*, 5952−5967.
(15) Zhulina, E. B.; Borisov, O. V. *Macromolecules* **2000**, *33*, 4945−4953.
(16) Csajka, F. S.; Netz, R. R.; Seidel, C.; Joanny, J.-F. *Eur. Phys. J. E* **2001**, *4*, 505−513.

(17) Naji, A.; Netz, R. R.; Seidel, C., submitted to *Eur. Phys. J. E*.
(18) Granfeldt, M. K.; Miklavic, S. J.; Marčelja, S.; Woodward, C. E. *Macromolecules* **1990**, *23*, 4760−4768.
(19) Sjöström, L.; Åkesson, T.; Jönsson, B. J. *J. Chem. Phys.* **1993**, *99*, 4739−4747.
(20) Chen, H.; Zajac, R.; Chakrabarti, A. *J. Chem. Phys.* **1996**, *104*, 1579−1588.
(21) Csajka, F. S.; van der Linden, C. C.; Seidel, C. *Macromol. Symp.* **1999**, *146*, 243−249.
(22) Csajka, F. S.; Seidel, C. *Macromolecules* **2000**, *33*, 2728−2739.
(23) Watanabe, H.; Patel, S. S.; Argillier, J. F.; Parsonnage, E. E.; Mays, J. W.; Dan-Brandon, N.; Tirrell, M. *Mater. Res. Soc. Symp. Proc.* **1992**, *249*, 255−265.
(24) Mir, Y.; Auvroy, P.; Auvray, L. *Phys. Rev. Lett.* **1995**, *75*, 2863−2866.
(25) Amiel, C.; Sikka, M.; Schneider, J. W.; Tsao, Y. H.; Tirrell, M.; Mays, J. W. *Macromolecules* **1995**, *28*, 3125−3134.
(26) Guenoun, P.; Schlachli, A.; Sentenac, D.; Mays, J. W.; Benattar, J. J. *Phys. Rev. Lett.* **1995**, *74*, 3628−3631.
(27) Ahrens, H.; Förster, S.; Helm, C. A. *Macromolecules* **1997**, *30*, 8447−8452; *Phys. Rev. Lett.* **1998**, *81*, 4172−4175.
(28) Tran, Y.; Auroy, P.; Lee, L.-T. *Macromolecules* **1999**, *32*, 8952−8964. Tran, Y.; Auroy, P.; Lee, L.-T.; Stamm, M. *Phys. Rev. E* **1999**, *60*, 6984−6990. Tran, Y.; Auroy, P. *Eur. Phys. J. E* **2001**, *5*, 65−79.
(29) Biesalski, M.; Rühe, J. *Macromolecules* **1999**, *32*, 2309−2313. Biesalski, M.; Rühe, J.; Johannsmann, D. *J. Chem. Phys.* **1999**, *111*, 7029−7037.
(30) Muller, F.; Fontaine, P.; Delsanti, M.; Belloni, L.; Yang, J.; Chen, Y. J.; Mays, J. W.; Lesieur, P.; Tirrell, M.; Guenoun, P. *Eur. Phys. J. E* **2001**, *6*, 109−115.
(31) Napper, D. H. *Polymeric Stabilization of Colloidal Dispersions*; Academic Press: New York, 1983.
(32) Park, Y. S.; Ito, Y.; Imanishi, Y. *Chem. Mater.* **1997**, *9*, 2755−2758. Ito, Y.; Park, Y. S.; Imanishi, Y. *Langmuir* **2000**, *16*, 5376−5381.
(33) Bell, G. I.; Dembo, M.; Bongrand, P. *Biophys. J.* **1984**, *45*, 1051−1064.
(34) Binder, K., Ed.; *Monte Carlo and Molecular Dynamics Simulations in Polymer Science*; Oxford University Press: New York, 1995.
(35) Dünweg, B.; Stevens, M. J.; Kremer, K. In ref 16, Chapter 3.3, pp 159−193.
(36) Murat, M.; Grest, G. S. *Macromolecules* **1989**, *22*, 4054−4059; *Phys. Rev. Lett.* **1989**, *63*, 1074−1077.
(37) Lekner, J. *Physica A* **1991**, *176*, 485−498.
(38) Sperb, R. *Mol. Simul.* **1994**, *13*, 189−193; *Mol. Simul.* **1998**, *20*, 179−200.
(39) Grest, G. S.; Kremer, K. *Phys. Rev. A* **1986**, *33*, 3628−3631.
(40) Allen, M. P.; Tildesley, D. J. *Computer Simulation of Liquids*; Oxford University Press: Oxford, 1987.
(41) Gropp, W.; Lusk, E.; Skjellum, A. *Using MPI*; The MIT Press: Cambridge, MA, 1994.
(42) Chandler, D. *Introduction to Modern Statistical Mechanics*; Oxford University Press: New York, 1987.
(43) Baigl, D.; Seery, T. A. P.; Williams, C. E. *Macromolecules* **2002**, *35*, 2318−2326.
(44) Humphrey, W.; Dalke, A.; Schulten, K. *J. Mol. Graphics* **1996**, *14*, 33−38.
(45) Moreira, A. G.; Netz, R. R. *Eur. Phys. J. E* **2002**, *8*, 33−58.
(46) Helm, C. A., private communication.

MA021428G